Prediction of Electron Densities, the Respective Laplacians, and Ellipticities in Bond-Critical Points of Phenyl−CH−Bonds via Linear Relations to Parameters of Inherently Localized CD Stretching Vibrations and ^{1}H NMR-Shifts

Martin Presselt,[†] Christoph Schnedermann,[†] Michael Schmitt,[†] and Jürgen Popp*[,†,‡]

Institute of Physical Chemistry, Friedrich-Schiller-University Jena, Helmholzweg 4, 07743 Jena, Germany, and Institute of Photonic Technology, Albert-Einstein-Str. 9, 07745 Jena, Germany

Received: October 30, 2008; Revised Manuscript Received: December 19, 2008

Electron densities ρ, the respective laplacians $\nabla^2\rho$, and ellipticities ϵ in bond-critical points (BCPs) are reactivity-determining characteristics according to the theory of atoms in molecules. These quantities are experimentally detectable only for substances in the crystalline state. To facilitate the determination of ρ, $\nabla^2\rho$, and ϵ values of BCPs of dissolved or liquid substances, the relations between DFT-calculated ρ, $\nabla^2\rho$, and ϵ and DFT-calculated vibrational and ^{1}H NMR spectroscopic quantities were studied for a set of 18 monosubstituted benzene derivatives. We found that via linear functions of ρ, $\nabla^2\rho$, or ϵ reliable predictions of ρ, $\nabla^2\rho$, and ϵ are possible, dependent on at least one of the variables vibrational transition energy, IR intensity, Raman activity of an inherently localized CD-stretching vibration, and the ^{1}H NMR shift. For the determination of ρ, $\nabla^2\rho$, and ϵ values in the ph−CH BCPs, the most important variables are the vibrational transition energy of the CD-stretching vibration and the corresponding ^{1}H NMR shift. The parameters of the functions best suited to predict ρ, $\nabla^2\rho$, and ϵ in the certain CH BCPs of the phenyl ring are presented.

Motivation and Approach

One of the most important topics in physical chemistry is the prediction of reactivity properties of molecules. One approach to determine molecular properties is to analyze the molecular electron density ρ distribution $\rho(r)$. According to the Hohenberg−Kohn−Theorem[1] (Nobel prize awarded to Walter Kohn in 1998, together with John Pople), molecular properties, like the reactivity, can be derived from the ρ distribution. The positions of the nuclei are determined by the maxima in $\rho(r)$, and also the nuclear charges can be derived from the gradient of ρ at the positions of the nuclei. Hence, the external potential can be calculated from the ρ distribution and the total number of electrons can be calculated by integrating $\rho(r)$ over the molecular space. With it, one can derive the molecular wave function based on $\rho(r)$ and can calculate the property of interest.

In the past few, years the experimental ρ determination by means of high-resolution X-ray measurements has drawn much attention, since technical improvements permit ρ determinations with justifiable effort and time consumption.[2−7] These experimental investigations of $\rho(r)$ have led to a paradigm shift in describing chemical bonding situations toward characterizing molecular key regions by means of their electron density features. Recently, $\rho(r)$ studies have been also successfully applied in the life sciences,[8−10] where the crystal site environments is supposed to represent the intermolecular interactions present under physiological conditions.[2] However, $\rho(r)$ of macromolecules, such as proteins or polynucleotides, can be only determined experimentally for special cases[2,11,12] because experimental $\rho(r)$ studies are generally linked to high-quality single crystals. Experimental $\rho(r)$ studies cannot be applied for substances that do not tend to form single crystals or of substances in various noncrystalline environments. For example, in life-sciences it would be of high interest to get information about $\rho(r)$ of a pharmaceutically active molecule in a physiological environment just before acting, or even more ambitious, to trace $\rho(r)$ during the mode of action of a molecule. Even there are ongoing efforts to make experimental $\rho(r)$ studies a routine application in the life sciences;[2,13−20] the latter tasks necessitate alternative approaches.

A possible alternative to high-resolution X-ray crystallography to study $\rho(r)$ characteristics, also of substances in various physical states, is the application of spectroscopic techniques to determine quantities related to $\rho(r)$ features. In the past, spectroscopic methods like for example vibrational and NMR spectroscopy applicable to molecules in different physical states were applied to conclude on $\rho(r)$-dependent molecular properties.[21] Thereby, the key question is always how to unravel the correlation between the spectroscopic data and the ρ distribution. Kagiya et al.[22] for example derived a simple relation between the relative electron-donating or -accepting nature of organic compounds and the IR−wavenumber positions of O−D or the C═O stretching bands of deuterated methanol or acetophenone. A frequently used approach to characterize reactivity, being a direct consequence of the respective ρ-distribution, is by means of the Hammett parameter σ, which is based on reaction rate constants.[23−25] Hansch et al. summarized the extensive work dealing with the application and refinement of the Hammett equation.[26] Several studies dealt with the electronic effects of substituents on the ρ distribution of benzene derivatives via Hammett parameters based on NMR data.[27,28] Dailey et al. found a linear correlation of ρ in the para position of differently substituted benzenes and the corresponding ^{1}H NMR shift compared to unsubstituted benzene.[29] In further studies, also the influence of neighboring atoms was taken into account.[30] Another possibility to calculate particular Hammett parameters describing the substituent effects on $\rho(r)$ is by using vibrational data. Brownlee and co-workers for example correlated the squared resonance substituent constant σ_R° with the IR intensity

[†] Friedrich-Schiller-University Jena.
[‡] Institute of Photonic Technology.

10.1021/jp809601a CCC: $40.75
Published on Web 03/06/2009

of certain normal modes.[31−34] Schmid et al. found that the IR intensity of aromatic C−H stretching modes are directly related to the Taft substitution constant σ_I.[35−40] Furthermore, a comparison between NMR- and IR-derived substituent resonance effect constants was performed by Palat et al.[41] Bobowitsch et al. pointed out how Raman intensities correlate with the Hammett parameter.[24,42−45] Bader and Chang studied the reactivity properties of substituted benzenes on the basis of the quantum theory of atoms in molecules (QTAIM) analyzing the topology of $\rho(r)$.[46−49] These studies revealed that the π populations and the quadrupole moments of the ring carbon atoms and the ellipticities of the phenyl C−H bonds are responsible for the reactivity in electrophilic aromatic substitution reactions.[50,51]

We have recently shown that certain differences in $\rho(r)$ between two related organic molecules manifested in the properties of the critical points (CPs) can be correlated with changes in the corresponding Raman spectra.[52] Hence, it is suggestive to study the relation between vibrational and NMR data and direct electron density features, like the properties in CPs. In doing so, it would be possible to express reactivity properties in terms of $\rho(r)$ features, providing an unambiguous scale, on the basis of spectroscopic data and without the limitation to single crystals. Here, we've chosen a set of monosubstituted benzene derivatives to investigate how $\rho(r)$ of the common substructure, the phenyl ring, is influenced by the different substituents and how the corresponding spectroscopic data are changing. Because to date it is impossible to get numerous single-crystal electron density data to perform such a statistical approach, we based our study on calculated electron density data and on calculated spectroscopic properties so far.

Calculation of Electron Density Properties

The two generally used schemes to compute electron density properties are based either on the partitioning of the wave function or on the real space partitioning of the electron density distribution. The by far most frequently applied representative of wave function-based partitioning schemes is the one of Mulliken,[53−56] whereas one of the real space electron density distribution partitioning schemes is Bader's quantum theory of atoms in molecules (QTAIM)[46−49] gaining in importance in the last years. Meister and Schwarz[21] published a comparative review about this topic. In contrast to properties derived from calculations based on the partitioning schemes of Mulliken and related approaches,[53−56] the QTAIM results are known to be less basis-set dependent.[3,4,21,57] Furthermore, AIM charges were found to be rather independent of the theoretical method used for computation, even if they are expected to exaggerate the real atomic charges, because a high density offloads the zero flux surface.[3,57,58] A study of Gomes et al. shows that the AIM charges give rise to good performances in calculating IR intensities comparable to ChelpG charges but are more consistent with the chemical experience based on the electronegativity concept than ChelpG charges.[59] Hence, $\rho(r)$ features determined by using the QTAIM are appropriate for quantum mechanical studies in context with vibrational investigations. In this study, we used ρ, the respective laplacians $\nabla^2\rho$, and the ellipticities ϵ in the bond-critical points (BCPs) of the phenyl−CH bonds to characterize the electron density distribution within the CH bonds.

The geometry optimizations, the computations of vibrational, and the NMR data were performed using the program *Gaussian 03* (*g03*),[60] applying two different theoretical levels. On the one hand, we applied the pure density functional of Becke and Perdew BP86[61,62] and the triple-ξ basis set TZVP[63,64] (polarization function on all atoms) known to give accurate molecular structures, frequencies, and Raman intensities for medium sized molecules.[65,66] On the other hand, we used the MP2[67] method in combination with the triple-ξ basis set 6-311+G(3df),[68−73] which is known to give reliable electron density values for BCPs.[57] The geometry optimization procedures in g03 were performed under *tight* and partially *verytight* (in conjunction with an *Ultrafine* grid) optimization conditions, to get reliable electron density characteristics, subsequently calculated with the program *AIM2000*.[74,75]

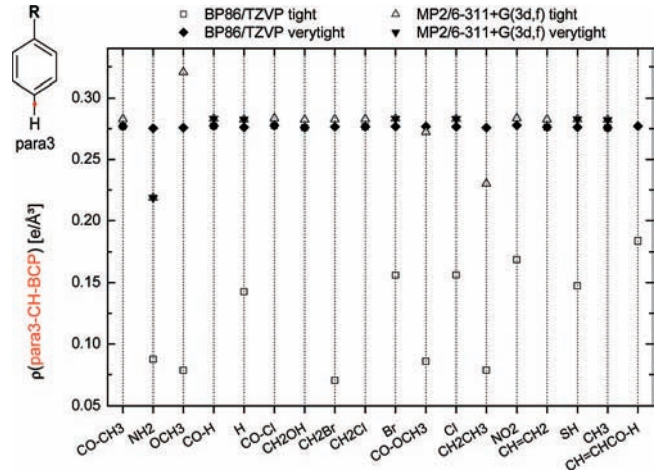

Figure 1. ρ in the BCPs of the *para*-CH bonds of all calculated benzene derivatives. Empty and filled dots: results obtained under *tight* and *verytight* optimization conditions, respectively. Squares and triangles correspond to BP86/TZVP and MP2/6-311+G(3df) calculations, respectively.

Figure 1 compares the BP86/TZVP and MP2/6-311+G(3df) calculated ρ values in the BCPs of the *para*-CH positions of a set of monosubstituted benzene derivates. The *tight* optimization condition (default grid) leads for the BP86/TZVP calculations to strongly divergent results, whereas for the *verytight* optimization condition (*Ultrafine* grid) the results are consistent. This behavior cannot be found for the MP2/6-311+G(3df) calculations. It can be seen in Figure 1 that for aniline, benzaldehyde, benzene, bromo-, and chloro-benzene, thiophenole, and toluole ρ does not differ noteworthy between the MP2/6-311+G(3df) calculations under *tight* and *verytight* conditions (default and *Ultrafine* grids, respectively). Hence, the *tight* optimization condition is sufficient to get reliable ρ, for the MP2/6-311+G(3df) approach. The corresponding densities are usually about 0.006 e/Å^3 higher than for the BP86/TZVP calculated ones, with the exception of R = OCH_3 (anisole) with an about 0.45 e/Å^3 higher ρ(*para*-CH BCP) and R = NH_2, $COOCH_3$, or CH_2CH_3 (aniline, benzoic-acid-methylester, ethyl-benzene) with a lower ρ(*para*-CH BCP). Generally the values calculated using MP2/6-311+G(3df) (*tight*) are spread over a wider range than the ones calculated applying BP86/TZVP (*verytight*). The MP2 calculations were performed in the default mode, that is using "frozen cores", that is the inner shells are not involved in the correlation calculation. In some MP2 geometry optimizations, we switched from the default Berny- to the GDIIS-optimizations to achieve convergence.

For a comparison of ρ of the four remaining CH BCPs of the phenyl group, one has to account for the computational limitation to fixed structures, for which reason the two sides of the phenylene group (ortho 1/5, meta 2/4) are differently affected by asymmetric substituents like for example CO−Cl (Figures 2 and 3). Consequently, different ρ values are obtained for the

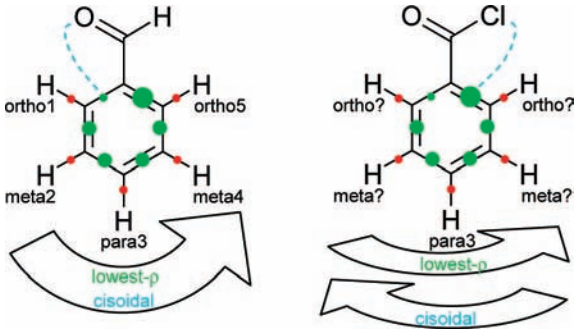

Figure 2. Illustration of the lowest-ρ- and the cis convention illustrated for the example of benzaldehyde (both conventions are leading to identical data sets) and benzoyl chloride (conventions are leading to inverse data sets). Magnitudes of ρ in the CC BCPs are indicated by the size of the green dots. Red dots indicate CH BCPs. The cyan dashed line points up the determination of the start CC bond according to the cis convention.

different ortho and meta positions and for the CC bonds on the different ph sides, respectively. Hence, to decide which sides of different benzene derivatives to compare, conventions are needed. One possibility is to apply a cis convention (Figure 2), where the data are collected starting at the ph−CC bond or ph−CH bond cisoidal to the β-substituent atom with the highest atomic number, going away from the substituent and ending up at the ph−CC bond transoidal to the substituent atom with the highest atomic number. Alternatively, we applied the lowest-ρ-convention (Figure 2), where the name indicates the starting point of the data collection, what is the only difference to the cis convention. The starting point is defined by the ph−CC bond with the lowest ρ in the BCP, adjacent to the ph−R bond. The properties of the CH bonds are collected according to the direction defined by ρ of the ph−CC bonds, regardless of ρ in the BCPs of the ph−CH bonds. The two conventions are compared in Figure 2. In the left graph, the example benzaldehyde is given, where the two conventions lead to equivalent data sets, because the start CC bonds are identical. In benzaldehyde, the substituent atom with the highest atomic number is oxygen. Hence, the adjacent CC bond is the starting point for the cis convention. The lower ρ in the BCP of the start CC position, according to the lowest-ρ-convention, is visualized by a smaller green dot in the CC bond compared to the end-CC position. In the case of benzoyl chloride, shown on the left side of Figure 2, the two conventions are leading to different orders of the ph−CH properties. According to Figure 2, the lowest-ρ-convention collects the data in the same direction like in the example of benzaldehyd but in benzoyl chloride the substituent atom with the highest atomic number is not oxygen anymore, but the chlorine atom. For that reason, the collection of data is performed in the opposite direction applying the cis convention, compared to the lowest-ρ-convention.

The sequences obtained from either convention, based on the ph−CC bonds, provide the basis for all of the data sets used in this work. The two conventions lead to equivalent assignments of ortho and meta positions with the exception of acetophenone and benzoyl chloride. The ρ values in the ortho and meta positions calculated under *tight* and *verytight* geometry-optimization conditions, based on the lowest-ρ-convention, are compared in Figures 1 and 2 of the Supporting Information. In Figure 3, ρ, $\nabla^2\rho$, and ϵ in the BCPs of all phenyl−CH positions are compared. The electron densities shown there were calculated under *verytight* geometry-optimization conditions using BP86/TZVP and applying the lowest-ρ-convention. As is expected, the *ortho*-CH BCPs are most affected by the inductive substituent effects, which can be seen from the large data range of ρ, $\nabla^2\rho$, and ϵ for the *ortho*-CH BCPs in Figure 3. The fact that, for example in benzoyl chloride, anisole and aniline ρ in the BCP of the *para*-CH bond is stronger influenced by the substituent than ρ in the BCP of the *meta*-CH bond can be explained by mesomeric effects. That the latter plays an important role is suggested by the great influence of the substituents on the ellipticities in the BCPs of the *para*-CH bonds. The ϵ (*para*-CH BCP) bonds are differing by the same

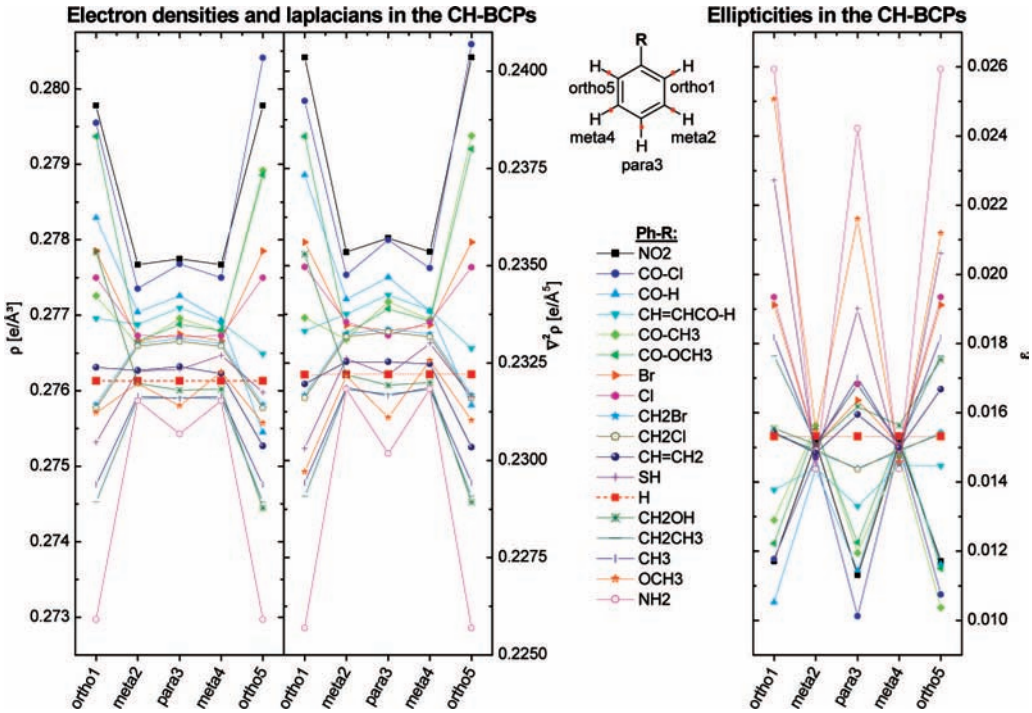

Figure 3. Electron densities (left), the respective laplacians (middle), and ellipticities (right) in the BCPs of the CH bonds of the phenyl group, according to the lowest-ρ-convention.

amount as the ellipticities within the *ortho*-CH bonds, whereas the ellipticities in the BCPs of the *meta*-CH bonds are less affected. The largest decrease of the ρ and $\nabla^2\rho$ values in the CH BCPs is observed for aniline, whereas the largest increase of ρ and $\nabla^2\rho$ of the CH BCPs can be found for nitrobenzene and benzoyl chloride. The NH_2 group (aniline) and the methoxy group (anisole) are leading to the highest ellipticities in the *ortho*- and *para*-CH BCPs, whereas the different ρ, $\nabla^2\rho$, and ϵ values in the *ortho*-CH BCPs of anisole highlight the different influence of asymmetric substituents on the different phenyl sides, as shown in Figure 3. The lowest ϵ values for the CH BCPs can be found for nitrobenzene, benzoylchloride, and benzaldehyde. Hence, to manipulate phenyl−CH-bond properties, the most effective way is to place NO_2, COCl, or NH_2 substituents in the ortho positions or, if the ortho positions are not accessible, in the para positions.

Calculation of Vibrational Data and NMR Shifts. As described in the previous section, we calculated ρ values in the BCPs, which are unambiguously related to the respective bonds. Because one aim of this study is the connection of these localized target quantities with vibrational data, it is necessary to also use localized vibrational data. Usually, this is not the case for normal modes (NM) even if certain phenyl NMs, like the trigonal ring breathing vibration of mono- or meta-substituted benzenes, are known to be substituent-independent because substituent motions are not involved in the vibrational mode, and neither of these NMs is strictly located to a single bond.

One way to overcome this problem is to consider monodeuterated benzene derivatives. The substitution of a single phenyl−hydrogen leads to a strong localized carbon−deuterium stretching vibration ν(CD), which can be found in a well separated wavenumber region of about 2300 cm^{-1}. Consequently, the stretching vibration of a given CD bond does not mix with other vibrations and is thus well located. The chemical properties of the CD bond are expected to be equal to the ones of a C−H bond. Hence, we use the vibrational characteristics of ν(CD) for a correlation with the ρ properties of the CH bonds. In the case of symmetric substituents (Br, Cl, NH_2, NO_2, CH_2Br, CH_2Cl, H, CH_2CH_3, CH_3) and ρ distributions, three Raman as well as IR spectra were calculated for ortho-, meta-, and para-deuteration, respectively. In the case of asymmetric substituents (CO−Cl, CO−H, CH═CHCO−H, CO−CH_3, CO−OCH_3, CH═CH_2, SH, CH_2OH, OCH_3) and ρ-distributions, five Raman and IR spectra were calculated for every monosubstituted benzene derivative, respectively. The corresponding Raman and IR data can be found in the Supporting Information.

To be consistent with the calculations of the density properties and following the work of Reiher et al.,[66] the vibrational data were calculated applying BP86/TZVP and *g03* simply involving the keyword *freq = Raman* (previous section). As a starting point, we used the pure Raman activities, as computed in the standard procedure of *g03*,[76] for our correlations. To relate the study to experimental investigations, the combinations of spectroscopic variables leading to the best fit results were reinvestigated by applying *relative* wavenumbers, IR intensities, and Raman intensities using benzene as standard. The relative wavenumbers were calculated as differences to the one of the CD-stretching vibration of benzene; relative IR and Raman intensities were normalized to the vibration of benzene. Raman intensities were calculated from Raman activities according to Schrötter and Klöckner assuming 293.15 K and an excitation wavelength of 752.488 nm.[77,78]

The chemical shifts of the phenyl−^{1}H ($\sigma^{1H}_{C_6H_6}$) were calculated using the gauge-independent atomic orbital (GIAO) method[79−83] and subtracting the resulting isotropic shielding value of ^{1}H of the various benzene derivates from the respective value of benzene. The NMR calculations are based on the ones of the Raman data, that is employing DFT[84,85] (BP86/TZVP), performing single point computations (involving the checkpointfile of the geometry optimization and Raman calculations).

Prediction of Electron Density Features Utilizing Spectroscopic Data. In a first attempt, we calculated linear correlation coefficients to test for linear relationships between spectroscopic variables, like the vibrational wavenumbers, IR intensities, Raman activities and ^{1}H NMR-shifts, and properties of the ρ-distributions of the CH bonds, like ρ, $\nabla^2\rho$, and ϵ within the CH BCPs. Furthermore, we applied the different data set generation conventions (lowest-ρ and cis convention) to decide which convention is preferable. In a next step, we are using linear and quadratic fit functions for ρ, $\nabla^2\rho$, and ϵ in the CH BCPs to test them for their ability to predict ρ, $\nabla^2\rho$, and ϵ values in the CH BCPs of unknown benzene derivatives.

Linear Correlation Coefficients. The linear correlation coefficients r were calculated according to eq 1, where the differences of the spectroscopic data x, as well as the $\rho(r)$ data f with their respective mean-values ($\bar{x}$,$\bar{f}$) are regarded.[86,87] The quantity n is the number of substances studied within this work.

$$r_{xf} = \frac{\frac{1}{n}\sum_{i=1}^{n}(x_i - \bar{x})(f_i - \bar{f})}{\sqrt{\frac{1}{n}\sum_{i=1}^{n}(x_i - \bar{x})^2}\sqrt{\frac{1}{n}\sum_{i=1}^{n}(f_i - \bar{f})^2}} \quad (1)$$

For the spectroscopic variable x, the chemical shifts ($\sigma^{1H}_{C_6H_6}$, described in the last section) of the phenyl protons, the wavenumber values of ν(CD), (WN), and the associated IR intensities (IR) and Raman activities (RA) were used. For the $\rho(r)$ data (f), ρ,$\nabla^2\rho$, and ϵ in the BCP of the phenyl−CH bond were chosen, respectively. The calculated correlation coefficients r are plotted in Table 1 for all combinations of spectroscopic quantities and $\rho(r)$-target quantities corresponding to the respective positions of the phenyl ring and to both data conventions (except for $\nabla^2\rho$, ϵ), described above.

From the data in Table 1, it can be concluded that there are no significant differences between both conventions in its correlation performance. We decided to use in the following the lowest-ρ convention due to an easier data handling.

The data in Table 1 suggest that the spectroscopic data, especially wavenumber values and IR intensities of highly localized ν(CD) and $\sigma^{1H}_{C_6H_6}$, are very strong linearly correlated to the electron density in the BCP of the CH bonds for certain positions of the monosubstituted benzene rings. The pairs of variables (i.e., spectroscopic variable and ρ, $\nabla^2\rho$, or ϵ) leading to absolute values of linear correlation coefficients higher than 0.75, indicating a very strong linear correlation, are highlighted bold in Table 1. The para position is the only CH position, which leads to weak linear correlations between the vibrational variables and ρ. Fortunately, this negligible linear correlation between the vibrational variables and ρ in the *para*-CH BCP is in contrast to the strong linear correlation of ρ with $\sigma^{1H}_{C_6H_6}$ in the *para*-CH BCP. A strong linear correlation between ρ and $\sigma^{1H}_{C_6H_6}$ is also present for the *ortho*-CH positions. Hence, the vibrational variables WN and IR as well as $\sigma^{1H}_{C_6H_6}$ are well suited to conclude from these spectroscopic data to ρ within the BCPs of ph−CH bonds. Even if the linear correlation of the vibrational variables with ρ for the para position is weak, ρ at the *para*-CH BCP can be well described via the strong linear

TABLE 1: Correlation Coefficients *r* between Vibrational and $\rho(r)$ Data (Upper, Middle, and Lower Part: ρ, $\nabla^2\rho$, and ϵ in the C−H BCP, Respectively)[a]

		NMR	Vibrational Data		
ph pos.		σ^{1H}_{C6H6}	WN	IR	RA
		ρ(BCP)			
ortho1	lowest-ρ conv.	**0.83**	**0.88**	**−0.88**	*−0.58*
	cis conv.	**0.86**	**0.88**	**−0.89**	*−0.64*
meta2	lowest-ρ conv.	*0.64*	**0.98**	**−0.90**	*0.50*
	cis conv.	*0.65*	**0.98**	**−0.88**	0.27
para3		**0.81**	0.14	0.07	0.27
meta4	lowest-ρ conv.	*0.69*	**0.99**	**−0.85**	0.21
	cis conv.	*0.69*	**1.00**	**−0.86**	0.40
ortho5	lowest-ρ conv.	**0.90**	**0.90**	**−0.86**	*−0.82*
	cis conv.	**0.88**	**0.89**	**−0.84**	*−0.77*
		$\nabla^2\rho$(BCP)			
ortho1	lowest-ρ conv.	**0.85**	**0.84**	**−0.85**	*−0.52*
meta2	lowest-ρ conv.	*0.61*	**0.98**	**−0.90**	*0.52*
para3		**0.86**	0.05	0.15	0.33
meta4	lowest-ρ conv.	*0.66*	**0.99**	**−0.85**	0.23
ortho5	lowest-ρ conv.	**0.92**	**0.89**	**−0.85**	**−0.83**
		ϵ(BCP)			
ortho1	lowest-ρ conv.	**−0.95**	−0.34	0.47	0.44
meta2	lowest-ρ conv.	0.10	−0.05	−0.01	−0.44
para3		**−0.98**	0.35	*−0.52*	*−0.56*
meta4	lowest-ρ conv.	0.39	0.11	−0.30	−0.37
ortho5	lowest-ρ conv.	**−0.90**	−0.35	0.43	*0.68*

[a] Bold and italic values indicate strong to full and medium to strong correlations, respectively. NMR data are the isotropic proton shieldings relative to the value of benzene. The vibrational data WN, IR, RA are the wavenumber, the IR intensity, and the Raman activity corresponding to the vibrational transitions of the strongly localized C−D stretching vibration.

correlation to $\sigma^{1H}_{C_6H_6}$. Hence, vibrational and ^{1}H NMR data complement one another and are perfectly suited to conclude electron densities from spectroscopic data applicable to substances in the liquid state. Equivalent correlations were obtained for $\nabla^2\rho$.

For a better visualization of for example the correlation between WN and ρ for a certain ph−CH BCP and for a comparison of the substituent influence on the CH BCPs for the different phenyl positions, the devolutions of the ρ and the WN values of all ph−CH positions are plotted against the different substituents in Figure 4. The high correlation coefficients between ρ and WN for the *meta*-CH/CD positions are well reflected in Figure 4 because the characteristics of the WN graphs are fitting well to the characteristics of the corresponding ρ graphs. Furthermore, the correlation coefficients r(WN,ρ) for the ortho positions indicate a strong linear correlation, even if minor differences between the curve progression of the ρ and the WN graphs of the ortho positions (Figure 4) are observed. The curve progressions of the WN graphs for the para position do not correspond to the ones of the corresponding ρ graphs, even if the differences in the ρ as well as in the WN values between all derivatives are low compared to the ortho position. This leads to the bad correlation coefficient between the vibrational wavenumber and the electron density in the BCP of the *para*-CH bonds.

Comparing the correlation coefficients r between the spectroscopic quantities and the ellipticities in the different ph-CH BCPs, shown in Table 1, the only quantity yielding high absolute values of r, indicating a strong linear correlation to ϵ, is $\sigma^{1H}_{C_6H_6}$ for the protons in the ortho and para positions. In the meta2 and meta4 positions, $r(\sigma^{1H}_{C_6H_6}, \epsilon)$ is very weak to weak (Table 1). In the case of the meta2 position, the highest linear correlation with ϵ can be found for the Raman activity; however indicating only a weak to medium-strong linear correlation with ϵ. For the meta4 position, the weak linear correlation between $\sigma^{1H}_{C_6H_6}$ and ϵ is nevertheless the highest for this position ($r(\sigma^{1H}_{C_6H_6}, \epsilon) = 0.39$), followed by r(RA, ϵ) = −0.37 and r(IR, ϵ) = −0.30 with linear correlation coefficients of comparable magnitude. Because $\sigma^{1H}_{C_6H_6}$ and RA complement each other in the linear relation with ϵ, these spectroscopic quantities are expected to be the most important variables to predict ϵ in the BCPs of ph−CH bonds in linear fits.

Fit Procedures. In the former section, it was shown that ρ, $\nabla^2\rho$, and ϵ values for the different ph−CH BCPs can be described by certain spectroscopic variables via linear fit relations. For a quantitative conclusion from one or more spectroscopic variables to the ρ, $\nabla^2\rho$, and ϵ values, it is necessary to find appropriate functions, fitting the ρ,$\nabla^2\rho$, or ϵ values. In a first step, we fitted ρ, $\nabla^2\rho$, and ϵ linearly dependent on each spectroscopic variable ($\sigma^{1H}_{C_6H_6}$, WN, IR, RA), respectively. In a next step, we extended the dimension of the linear function subsequently to the fifths dimension by involving additional spectroscopic variables. In doing so, we considered all possible permutations in each dimension. Finally, we performed the same procedure for quadratic functions and identified the best methods to calculate ρ, $\nabla^2\rho$, and ϵ values.

All fits were performed for data sets build up according to the lowest-ρ convention and are based on either eqs 2 or 3. The target quantities ρ, $\nabla^2\rho$, and ϵ are denoted as f, whereas the different spectroscopic values WN, IR, and RA of the CD-bond stretching vibrations and $\sigma^{1H}_{C_6H_6}$ were chosen as variables (α, β, γ, δ) in the fit functions, that is eqs 2 and 3. The latin characters $a-p$ (except f) are the corresponding fit parameters. Eq 2 represents the linear fit functions, where the form with the highest dimension is shown. The quadratic fit function with the highest dimension (eq 3) includes linear, quadratic, and mixing terms.

$$f^{\mathrm{lin}}(\alpha,\beta,\gamma,\delta) = a + b\alpha + c\beta + d\gamma + e\delta \qquad (2)$$

$$f^{\mathrm{quad}}(\alpha,\beta,\gamma,\delta) = f^{\mathrm{lin}}(\alpha,\beta,\gamma,\delta) + g\alpha^2 + h\beta^2 + i\gamma^2 + j\delta^2 + k\alpha\beta + l\alpha\gamma + m\alpha\delta + n\beta\gamma + o\beta\delta + p\gamma\delta \qquad (3)$$

The fit performance is evaluated by the sum of the squared errors χ^2 (eq 4) and by the validated sum of squared errors val-χ^2 (eq 5). In these equations, n is the number of substances studied within this work (also eq 1), f_i are the DFT calculated ρ, $\nabla^2\rho$, or ϵ values, f_{fit} are the corresponding fit function values, and f_{refit} is explained in the following.

$$\chi^2 = \sum_{i=1}^{n} (f_i - f_{\mathrm{fit}})^2 \qquad (4)$$

$$\mathrm{val}-\chi^2 = \sum_{i=1}^{n} (f_i - f_{\mathrm{refit}})^2 \qquad (5)$$

Val-χ^2 was calculated to estimate the capability of the fit function to predict ρ, $\nabla^2\rho$, or ϵ values of new substances, which were not considered in the fit. Therefore, each point within a fit is treated as unknown once, with subsequent refitting of the function for each omitted point. Refitting was done using all data points except of one, which was afterward predicted using the respective spectroscopic data as input. The sum of the squared differences of all in this way predicted values f_{refit}, and the corresponding DFT calculated values f_i is val-χ^2. Because

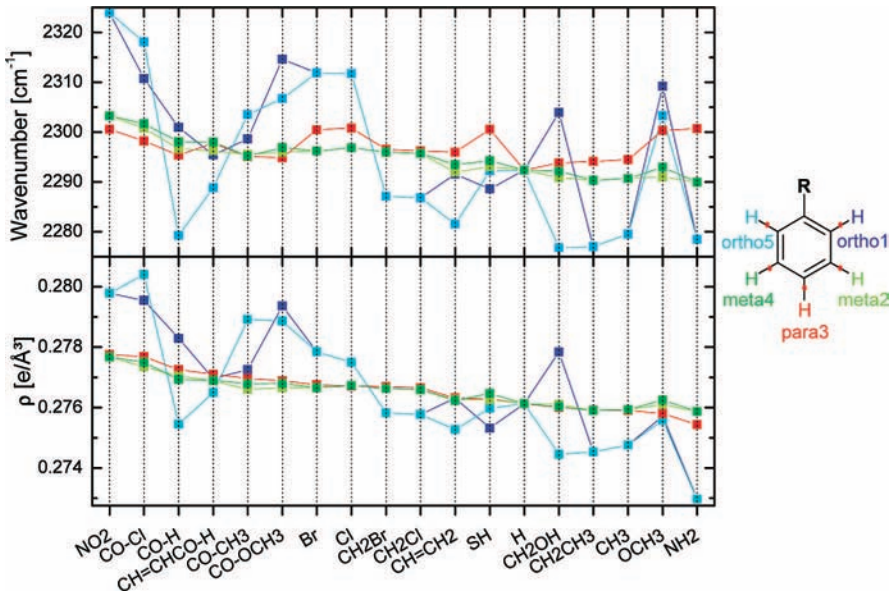

Figure 4. Comparison of the calculated ρ in the ph−CH BCPs and the corresponding CD-stretching vibrations for the different ph positions of all benzene derivatives studied within this work. The upper graph shows the wavenumbers of ν(CD) and the lower the corresponding ρ in the BCP(CH). The x axis is built with respect to a decreasing ρ in *para*-CH BCP from the left to the right.

the final goal is to predict electron density properties of new substances with unknown electron density distributions, we focus on this value for comparing different fits in the following.

Linear Fit Results of the Electron Densities for the ph−CH BCPs. The χ^2 and the val-χ^2 values of the linear fits of the electron densities depending on the spectroscopic variables are compared in the upper part of Table 2. For the ortho and para positions, the extension of the fit dimensionality from 2D to 3D results in a significant decrease of val-χ^2 of about one magnitude. Further enhancement of the dimensionality of the fit functions leads only to minor changes in val-χ^2. Because for the meta positions an almost perfect linear correlation between WN and the ρ values can be found, the consideration of additional spectroscopic variables does not lead to significant improvements in the fit performance. In the following, the different linear fits of the ρ values are compared with each other for each position to identify the best-fit procedure.

The highest val-χ^2 values are found for the linear fit dependent on one variable for the ortho positions. Different variables are leading to the best results of the linear 2D fits for the two ortho positions namely the IR intensity in the linear 2D fit of ρ for the *ortho1*-CH BCPs and $\sigma^{1H}{}_{C_6H_6}$ in the linear 2D fit of ρ for the ortho5 position. For both these ortho positions, a fit-dimensionality enhancement by using a further spectroscopic variable leads to a decrease of val-χ^2 of roughly one magnitude. It is surprising that the combination of variables leading to the lowest val-χ^2 in the linear 3D fits of ρ for the *ortho1*-CH BCPs does not involve the IR intensity but WN and $\sigma^{1H}{}_{C_6H_6}$. This also holds for linear 3D fits of ρ in *ortho5*-CH BCPs. A further extension of the dimensionality of the linear fit of ρ of the *ortho1*-CH BCPs by including the IR intensity leads only to a slight lowering of val-χ^2, whereas a subsequent extension by additionally using the Raman activity lowers the val-χ^2 value by about one-fifth. Equivalent results are obtained for ρ in the ortho5 positions, with the exception of the lowest and the highest dimensional linear fit. The linear fit of ρ(ortho5 BCP) with the lowest val-χ^2 depends on WN, IR, and $\sigma^{1H}{}_{C_6H_6}$.

For the meta2 and the meta4 positions, where correlation coefficients of roughly one were calculated for the linear relation between WN of ν(*meta*-CD) and ρ in the corresponding BCPs, very good 2D linear fits of ρ(BCP) dependent on WN are of course possible. Only slight improvements of the performance of the linear fits are observed by using additional variables, where the lowest val-χ^2 value for the meta2 position can be found if all three vibrational variables are included. For the meta4 position the linear fit of ρ depending on WN leads to the lowest val-χ^2. Furthermore, the same combinations of variables lead to the best linear fits of ρ for both meta positions in each dimension, respectively.

Considering the bad correlation for the para positions poor linear fits of ρ depending on the vibrational variables are expected for the para position. We found a strong linear correlation only between ρ(*para3*-CH BCP) and $\sigma^{1H}{}_{C_6H_6}$, indicated by the correlation coefficient of 0.81. Comparable results were obtained by Dailey et al., who found the ^{1}H NMR spectra of substituted benzenes to correlate reasonably well with the π-electron density in the para position.[29] Nevertheless, the application of WN and IR of ν(*para3*-CD) as additional variables to $\sigma^{1H}{}_{C_6H_6}$ leads to a significant lowering of val-χ^2 as compared to the linear 2D fit of ρ for the *para3*-CH BCP just depending on $\sigma^{1H}{}_{C_6H_6}$.

Quadratic Fit Results of the Electron Densities for the ph−CH BCPs. Because of the additional degrees of freedom, the quadratic fit functions (eq 3) lead to lower χ^2 values than the linear fit functions, which is shown in Table 2. Nevertheless, the quadratic functions are not automatically better suited to predict unknown ρ values than the linear functions as can be seen on the val-χ^2 values. There are only two cases (Table 2), where the quadratic fit yields a slightly lower val-χ^2 than the linear fits. These are the 3D and 4D quadratic fits of ρ in the *meta2*- and the *para3*-CH BCPs, respectively, labeled as bold underlined val-χ^2 values in Table 2. Thereby, ρ(*meta2*-CH BCP) in the quadratic fit depends on WN and $\sigma^{1H}{}_{C_6H_6}$ and ρ(*para3*-CH BCP) depends on WN, IR, and $\sigma^{1H}{}_{C_6H_6}$.

Figure 5 provides a graphical illustration of the fit results. The red dots display the input data for the fit derived from our DFT calculations that is WN, $\sigma^{1H}{}_{C_6H_6}$, and ρ for the *meta2*-CH BCP. The blue surface displays the fit function and the blue dots represent the fitted ρ values for the input WN and $\sigma^{1H}{}_{C_6H_6}$ data. For a perfect fit, the red and blue dots would match

TABLE 2: Sums of Squared Errors χ^2 and Validated Sums of Squared Errors val-χ^2 of the Fits of the Electron Densities in the BCPs of all ph−CH Bonds, Depending on the Spectroscopic Parameters WN, IR, RA, σ^{Ha}

χ^2 [e/Å^3] and val-χ^2 [e/Å^3] for ρ(BCP) Prediction, Based on Lowest ρ Convention										
variables	ortho1		meta2		para3		meta4		ortho5	
linear[b]	χ^2	val-χ^2	χ^2	val-χ^2	χ^2	val-χ^2	χ^2	val-χ^2	χ^2	val-χ^2
WN[c]	1.35×10^{-5}	1.70×10^{-5}	1.48×10^{-7}	$\mathbf{1.75 \times 10^{-7}}$	6.99×10^{-6}	8.98×10^{-6}	9.68×10^{-8}	$\underline{\mathbf{1.13 \times 10^{-7}}}$	1.34×10^{-5}	1.68×10^{-5}
IR[c]	1.31×10^{-5}	$\mathbf{1.65 \times 10^{-5}}$	8.52×10^{-7}	1.06×10^{-6}	7.10×10^{-6}	8.92×10^{-6}	1.28×10^{-6}	1.62×10^{-6}	1.80×10^{-5}	2.26×10^{-5}
RA[c]	3.88×10^{-5}	5.29×10^{-5}	3.24×10^{-6}	3.91×10^{-6}	6.62×10^{-6}	8.58×10^{-6}	4.32×10^{-6}	5.19×10^{-6}	2.21×10^{-5}	3.21×10^{-5}
σ^{Hd}	1.80×10^{-5}	2.37×10^{-5}	2.52×10^{-6}	3.17×10^{-6}	2.42×10^{-6}	$\mathbf{2.96 \times 10^{-6}}$	2.40×10^{-6}	2.97×10^{-6}	1.28×10^{-5}	$\mathbf{1.54 \times 10^{-5}}$
WN, IR	9.92×10^{-6}	1.52×10^{-5}	1.08×10^{-7}	$\mathbf{1.36 \times 10^{-7}}$	4.90×10^{-6}	6.92×10^{-6}	9.63×10^{-8}	$\mathbf{1.27 \times 10^{-7}}$	1.18×10^{-5}	1.63×10^{-5}
WN, RA	1.19×10^{-5}	1.62×10^{-5}	1.36×10^{-7}	1.83×10^{-7}	5.77×10^{-6}	8.29×10^{-6}	9.64×10^{-8}	1.33×10^{-7}	5.31×10^{-6}	1.00×10^{-5}
WN, σ^H	1.68×10^{-6}	$\mathbf{2.58 \times 10^{-6}}$	1.08×10^{-7}	1.51×10^{-7}	2.00×10^{-7}	$\mathbf{3.35 \times 10^{-7}}$	8.99×10^{-8}	1.41×10^{-7}	1.65×10^{-6}	$\mathbf{2.59 \times 10^{-6}}$
IR, RA	1.30×10^{-5}	1.92×10^{-5}	7.21×10^{-7}	1.27×10^{-6}	6.45×10^{-6}	8.80×10^{-6}	7.29×10^{-7}	1.11×10^{-6}	1.27×10^{-5}	2.10×10^{-5}
IR, σ^H	5.72×10^{-6}	7.88×10^{-6}	5.24×10^{-7}	7.42×10^{-7}	2.59×10^{-7}	3.96×10^{-7}	8.71×10^{-7}	1.19×10^{-6}	4.50×10^{-6}	6.17×10^{-6}
RA, σ^H	1.73×10^{-5}	2.72×10^{-5}	1.90×10^{-6}	2.60×10^{-6}	2.07×10^{-6}	2.84×10^{-6}	2.34×10^{-6}	3.27×10^{-6}	1.14×10^{-5}	1.83×10^{-5}
WN, IR, RA	9.87×10^{-6}	1.79×10^{-5}	1.03×10^{-7}	$\mathbf{1.31 \times 10^{-7}}$	4.71×10^{-6}	8.02×10^{-6}	9.65×10^{-8}	$\mathbf{1.44 \times 10^{-7}}$	5.23×10^{-6}	1.15×10^{-5}
WN, IR, σ^H	1.53×10^{-6}	$\mathbf{2.53 \times 10^{-6}}$	8.93×10^{-8}	1.40×10^{-7}	1.51×10^{-7}	$\mathbf{2.93 \times 10^{-7}}$	8.99×10^{-8}	1.55×10^{-7}	1.44×10^{-6}	$\underline{\mathbf{2.57 \times 10^{-6}}}$
WN, RA, σ^H	1.55×10^{-6}	2.58×10^{-6}	9.13×10^{-8}	1.68×10^{-7}	2.00×10^{-7}	3.87×10^{-7}	8.98×10^{-8}	1.65×10^{-7}	1.28×10^{-6}	3.26×10^{-6}
IR, RA, σ^H	4.75×10^{-6}	8.78×10^{-6}	4.08×10^{-7}	9.47×10^{-7}	2.34×10^{-7}	4.32×10^{-7}	5.17×10^{-7}	1.02×10^{-6}	4.47×10^{-6}	9.31×10^{-6}
WN, IR, RA, σ^H	1.17×10^{-6}	$\underline{\mathbf{2.02 \times 10^{-6}}}$	7.97×10^{-8}	$\mathbf{1.37 \times 10^{-7}}$	1.40×10^{-7}	$\mathbf{3.14 \times 10^{-7}}$	8.97×10^{-8}	1.82×10^{-7}	1.25×10^{-6}	3.93×10^{-6}
quadratic[e]										
WN	1.29×10^{-5}	$\mathbf{1.87 \times 10^{-5}}$	1.49×10^{-7}	$\mathbf{1.90 \times 10^{-7}}$	5.66×10^{-6}	9.00×10^{-6}	9.62×10^{-8}	$\mathbf{1.22 \times 10^{-7}}$	1.34×10^{-5}	$\mathbf{1.88 \times 10^{-5}}$
IR	1.27×10^{-5}	2.03×10^{-5}	8.38×10^{-7}	1.20×10^{-6}	4.84×10^{-6}	6.99×10^{-6}	1.24×10^{-6}	1.70×10^{-6}	1.64×10^{-5}	2.68×10^{-5}
RA	3.81×10^{-5}	8.17×10^{-5}	3.20×10^{-6}	4.05×10^{-6}	6.20×10^{-6}	9.10×10^{-6}	4.31×10^{-6}	6.63×10^{-6}	1.51×10^{-5}	3.80×10^{-5}
σ^H	1.68×10^{-5}	2.97×10^{-5}	2.13×10^{-6}	3.31×10^{-6}	2.10×10^{-6}	$\mathbf{4.20 \times 10^{-6}}$	2.33×10^{-6}	3.46×10^{-6}	1.28×10^{-5}	1.95×10^{-5}
WN, IR	9.32×10^{-6}	3.57×10^{-5}	1.03×10^{-7}	1.90×10^{-7}	2.87×10^{-6}	6.90×10^{-6}	7.94×10^{-8}	$\mathbf{1.31 \times 10^{-7}}$	1.09×10^{-5}	3.00×10^{-5}
WN, RA	1.18×10^{-5}	3.05×10^{-5}	1.05×10^{-6}	1.05×10^{-6}	4.53×10^{-6}	1.41×10^{-5}	8.99×10^{-8}	3.51×10^{-7}	3.77×10^{-6}	1.58×10^{-5}
WN, σ^H	1.23×10^{-6}	$\mathbf{4.71 \times 10^{-6}}$	7.12×10^{-8}	$\underline{\mathbf{1.25 \times 10^{-7}}}$	1.40×10^{-7}	4.86×10^{-7}	5.05×10^{-8}	1.59×10^{-7}	1.22×10^{-6}	$\mathbf{3.57 \times 10^{-6}}$
IR, RA	6.95×10^{-6}	4.08×10^{-5}	2.71×10^{-6}	2.71×10^{-6}	4.58×10^{-6}	1.04×10^{-5}	4.49×10^{-7}	2.00×10^{-6}	5.35×10^{-6}	2.97×10^{-5}
IR, σ^H	3.89×10^{-6}	1.20×10^{-5}	3.89×10^{-7}	7.00×10^{-7}	2.02×10^{-7}	$\mathbf{3.94 \times 10^{-7}}$	6.85×10^{-7}	1.25×10^{-6}	2.61×10^{-6}	5.97×10^{-6}
RA, σ^H	1.09×10^{-5}	4.10×10^{-5}	1.59×10^{-6}	4.98×10^{-6}	1.92×10^{-6}	6.20×10^{-6}	1.59×10^{-6}	1.05×10^{-5}	8.76×10^{-6}	3.91×10^{-5}
WN, IR, RA	2.93×10^{-6}	6.76×10^{-5}	9.07×10^{-8}	1.13×10^{-5}	1.63×10^{-6}	2.71×10^{-5}	5.78×10^{-8}	6.98×10^{-7}	1.66×10^{-6}	1.68×10^{-5}
WN, IR, σ^H	1.13×10^{-6}	3.77×10^{-5}	2.34×10^{-8}	$\mathbf{3.36 \times 10^{-7}}$	2.17×10^{-8}	$\underline{\mathbf{1.81 \times 10^{-7}}}$	2.94×10^{-8}	$\mathbf{2.98 \times 10^{-7}}$	6.70×10^{-7}	8.63×10^{-6}
WN, RA, σ^H	7.41×10^{-7}	1.24×10^{-5}	4.10×10^{-8}	1.39×10^{-6}	7.86×10^{-8}	6.81×10^{-7}	3.37×10^{-8}	3.40×10^{-7}	4.93×10^{-7}	$\mathbf{6.60 \times 10^{-6}}$
IR, RA, σ^H	1.29×10^{-6}	$\mathbf{7.63 \times 10^{-6}}$	1.19×10^{-7}	2.15×10^{-6}	1.13×10^{-7}	4.82×10^{-7}	8.63×10^{-8}	6.65×10^{-7}	1.44×10^{-6}	2.57×10^{-5}
WN, IR, RA, σ^H	2.02×10^{-7}	1.01×10^{-4}	6.50×10^{-9}	6.24×10^{-6}	1.32×10^{-8}	2.43×10^{-5}	3.63×10^{-9}	1.01×10^{-6}	3.68×10^{-7}	6.14×10^{-5}

[a] Bold values are the lowest within each fit dimension, and underlined values are the lowest val-χ^2 values at the respective position taking all corresponding fits into account. [b] Application of linear variables in the fit-functions according to eq 2. [c] Wavenumbers, IR intensities, and Raman activities of the ν(CD) modes. [d] NMR shift calculated by subtracting the isotropic ^{1}H-shielding value from the one of C_6H_6. [e] Application of linear and quadratic variables in the fit functions according to eq 3.

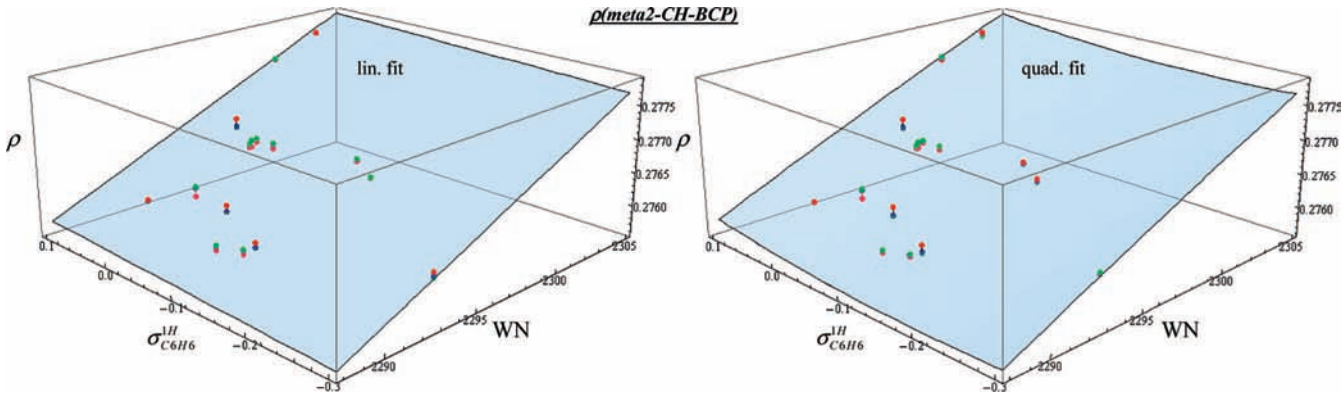

Figure 5. Graphical illustration of ρ(WN, $\sigma^{1H}_{C_6H_6}$) of the *meta2*-position: **left**: linear fit, **right**: quadratic fit; *dots*: red: DFT calculated, blue: fitted, green: predicted due to refitting; *surface*: fitted function based on all DFT-calculated data points.

perfectly. The green dots display via validated functions predicted ρ values. The quadratic fit function (blue surface right part of Figure 5) reveals that the quadratic terms contribute minor to the fit surfaces within the region the data points are spread over.

For most of the cases studied within this work (Table 2), the quadratic functions lead to higher val-χ^2 values than the linear functions. The reason for that is the stronger descent or ascent of the quadratic function away from the center of the data volume, which is illustrated in Figure 6 where the fit function (blue surface) is compared to a fit function based on the validated ρ values (green surface). The larger vertical distance of the val-χ^2 surface (green) to the DFT-fit surface (blue) at the edges for the quadratic fit compared to the linear fit highlights the bad prediction of points in the peripheral data regions, which are not planelike distributed, by applying a quadratic fit.

The global best fit concerning the prediction of unknown ρ(CH BCP), that is the fit with the lowest val-χ^2, was found to be the linear fit depending on WN at the meta4 position (val-χ^2 $= 1.1 \times 10^{-7}$ e/Å^3). The values for the slope and the intercept are 1.392×10^{-4} e/Å^3 and -0.043 cm $\times$ e/Å^3, respectively. Generally $\sigma^{1H}_{C_6H_6}$ and WN are the most important variables to predict ρ in the BCPs of ph−CH bonds, applying linear functions. This combination gives relatively low val-χ^2 values at all five ph−CH positions. The additional consideration of IR leads to slight improvements in the ρ-prediction performance,

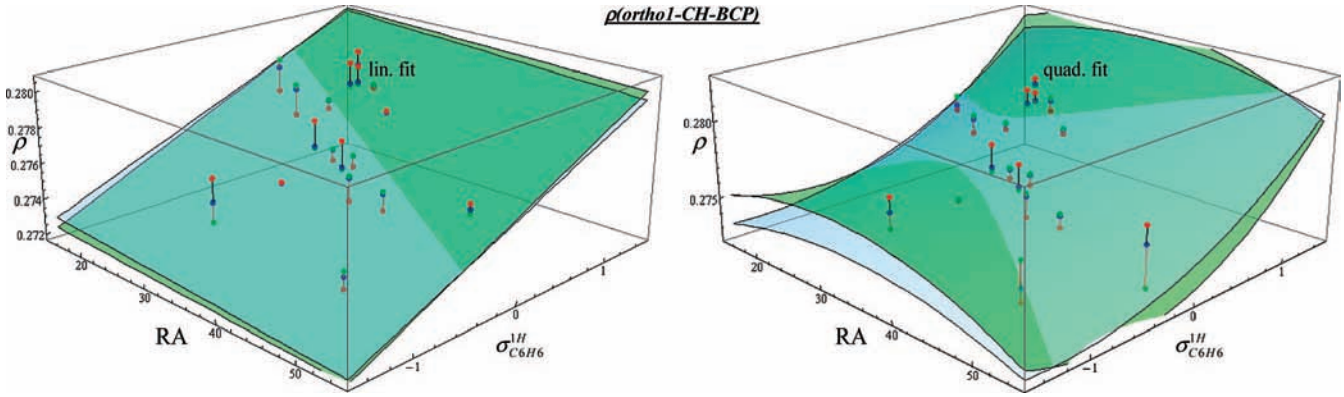

Figure 6. Graphical illustration of ρ(WN,RA) of the ortho1 position: **left**: linear fit, **right**: quadratic fit; *dots*: red: DFT calculated, blue: fitted, green: predicted due to refitting; *surfaces*: blue: fitted function based on all DFT-calculated data points, green: fitted function based on all predicted/refitted data.

TABLE 3: Parameters of the Best Linear Fit Functions of the Electron Densities in the BCPs for Each ph−CH Bond[a]

Fits of ρ(BCP) Based on Lowest ρ Convention and According to Eq *2*							
variables	1	σH	WN	IR	RA		
parameter	a	b	c	d	e	χ^2 [e/Å^3]	val-χ^2 [e/Å^3]
ortho1	0.1221	1.795×10^{-3}	6.708×10^{-5}	-1.395×10^{-4}	2.443×10^{-5}	1.17×10^{-6}	2.02×10^{-6}
	0.1131	1.694×10^{-3}	7.122×10^{-5}	-7.974×10^{-5}	0	1.53×10^{-6}	2.53×10^{-6}
	0.0876	1.796×10^{-3}	8.220×10^{-5}	0	0	1.68×10^{-6}	2.58×10^{-6}
meta2	−0.1079	0	1.671×10^{-4}	1.057×10^{-4}	4.884×10^{-6}	1.03×10^{-7}	1.31×10^{-7}
	−0.0806	3.424×10^{-4}	1.554×10^{-4}	8.336×10^{-5}	0	8.98×10^{-8}	1.40×10^{-7}
	−0.0107	4.690×10^{-4}	1.252×10^{-4}	0	0	1.08×10^{-7}	1.52×10^{-7}
para3	0.0783	2.731×10^{-3}	8.679×10^{-5}	-1.625×10^{-4}	0	1.51×10^{-7}	2.92×10^{-7}
	0.0783	2.731×10^{-3}	8.679×10^{-5}	-1.625×10^{-4}	0	1.51×10^{-7}	2.92×10^{-7}
	−0.0482	2.558×10^{-3}	1.415×10^{-4}	0	0	2.00×10^{-7}	3.35×10^{-7}
meta4	−0.0429	0	1.392×10^{-4}	0	0	9.68×10^{-8}	1.13×10^{-7}
	−0.0323	2.020×10^{-4}	1.346×10^{-4}	7.291×10^{-7}	0	8.99×10^{-8}	1.55×10^{-7}
	−0.0318	2.028×10^{-4}	1.343×10^{-4}	0	0	8.99×10^{-8}	1.41×10^{-7}
ortho5	0.1422	2.006×10^{-3}	5.857×10^{-5}	-8.149×10^{-5}	0	1.44×10^{-6}	2.57×10^{-6}
	0.1422	2.006×10^{-3}	5.857×10^{-5}	-8.149×10^{-5}	0	1.44×10^{-6}	2.57×10^{-6}
	0.1148	2.074×10^{-3}	7.039×10^{-5}	0	0	1.65×10^{-6}	2.59×10^{-6}

[a] In the first, second, and third row of each position, the parameters of the globally best linear fit and of the generally good fits ρ(WN, $\sigma^{1H}_{C_6H_6}$) and ρ(WN, $\sigma^{1H}_{C_6H_6}$, IR) are presented, respectively.

as the lower val-χ^2 values summed over all CH positions (5.65×10^{-6} e/Å^3) compared to the application of WN and $\sigma^{1H}_{C_6H_6}$ in the 3D fit (val-$\chi^2 = 5.82 \times 10^{-6}$ e/Å^3) reveals. The parameters of the globally best linear fit function and of the linear functions ρ(WN,$\sigma^{1H}_{C_6H_6}$) and ρ(WN,$\sigma^{1H}_{C_6H_6}$,IR) to predict the ρ values in the BCPs of each ph−CH position are summarized in Table 3.

To further assess the performance of predicting ρ values in ph−CH bonds on the basis of the fit functions presented in Table 3 the DFT-calculated, the fitted, and the validated ρ values corresponding to the best linear ρ fits (Table 3) are depicted in Figure 7. The upper graph shows ρ in the *ortho*-CH BCPs, the middle and the lower graph show ρ in the *meta*- and *para*-CH BCPs, respectively. For the ortho and meta graphs, the left and the right side of the columns corresponds to the ortho1, ortho5, meta2, and the meta4 positions, respectively. As illustrated by Figure 7, applying the fitted functions presented in eq 2 and Table 3, it is possible to predict the electron density in the BCPs of ph−CH bonds quite accurately, which enables a classification of unknown ρ on the basis of spectroscopic data.

Linear and Quadratic Fit Results of the Laplacians $\nabla^2\rho$ for the ph−CH BCPs. The laplacians are especially sensitive to reactivities, and hence we studied if we can translate the relations derived for ρ onto the laplacian. As can be seen in Figure 3, the laplacian values are distributed in a similar way to the electron density values in the CH BCPs. Consequently, a similar prediction performance is expected. In Table 4, the χ^2, val-χ^2 values, and the parameters of the best fits are presented. Table 2 within the supplementary section displays the performance of all studied fits. Table 4 reveals that the val-χ^2 values are roughly a half-magnitude higher than the best fits of ρ because the $\nabla^2\rho$ values are covering a significant larger data range. To visualize the excellent fit results, the DFT-calculated, the fitted, and the validated laplacians are plotted in Figure 8.

Linear and Quadratic Fit Results of the Ellipticities ϵ for the ph−CH BCPs. The same procedure as described above for the prediction of electron density values was applied to study the relation between the spectroscopic variables and ϵ. The corresponding results for the ϵ fit are summarized in Table 2 of the Supporting Information. As already suggested by the correlation coefficients plotted in Table 1, the most important variables to predict ϵ in the BCP of a ph−CH bond in a 2D linear fit are $\sigma^{H}_{C_6H_6}$ and RA, leading to the lowest val-χ^2 values in the ortho/para and meta positions, respectively. The low val-χ^2 values for the meta positions compared to the other CH positions are simply due to the small changes of ϵ between all benzene derivatives at the meta positions as visualized in Figure 9, where the DFT-calculated ϵ values and the ones corresponding to the best fit (lowest val-χ^2) for each phenyl position are depicted. The respective parameters of the best fits are presented in Table 5.

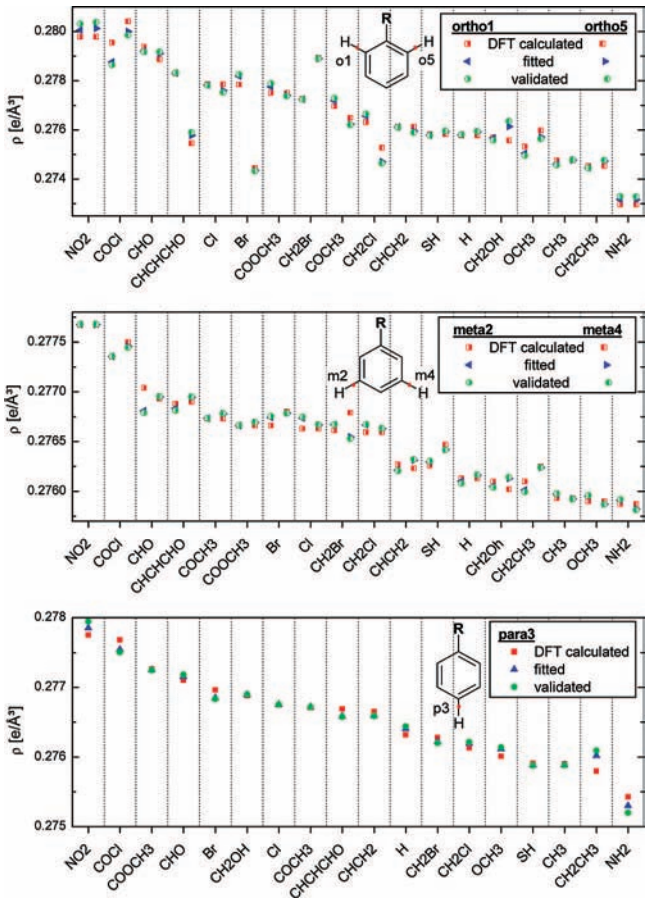

Figure 7. DFT-calculated, fitted, and validated ρ values in the BCPs of the CH bonds. The fit functions are linear and the parameters are the ones leading to the lowest val-χ^2 shown in Table 3.

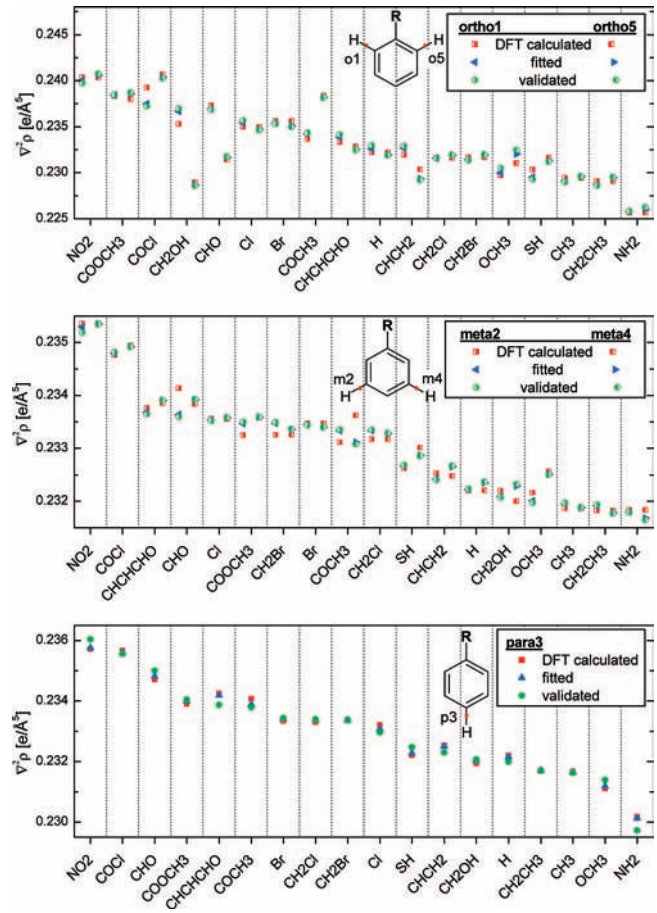

Figure 8. DFT-calculated, fitted, and validated $\nabla^2\rho$ values in the BCP of the CH bonds. The fit functions are linear, and the parameters are the ones leading to the lowest val-χ^2 in Table 4.

For the ortho1 position, the linear function $\epsilon(\sigma^{1H}_{C_6H_6}, WN)$ possesses the lowest val-χ^2. The respective fit for the ortho5 position is of comparable performance, even if the application of the IR intensity instead of the WN ($\epsilon(\sigma^{1H}_{C_6H_6}, IR)$ quadratic function) leads to a somewhat lower val-χ^2 for a quadratic fit function. In general, ϵ can be well predicted by means of WN and $\sigma^{1H}_{C_6H_6}$ as can be seen in Figure 9. For ϵ in the *meta2*-CH BCP, the best results are obtained by involving Raman activities in the case of linear fits, as suggested by the correlation coefficients summarized in Table 1. The inclusion of additional variables does not improve the fit. Nevertheless, for ϵ in the *meta2*-CH BCP, the lowest val-χ^2 is found for the quadratic dependence of ϵ on $\sigma^{1H}_{C_6H_6}$. For ϵ in the *meta4*-CH BCP, the best fit is obtained for a linear function by using all spectroscopic variables, except the Raman activity. The precision in predicting ϵ in the meta positions is higher than for all other positions, though an arrangement of predicted ϵ values in an order of known substances is quite challenging due to the low differences

TABLE 4: Parameters of the Best Linear Fit Functions of the Laplacians of the Electron Densities in the BCPs for Each ph−CH Bond

Fits of $\nabla^2\rho$(BCP) Based on Lowest ρ Convention and According to Eq *2*							
variables	1	σH	WN	IR	RA		
parameter	a	b	c	d	e	χ^2 [e/Å^5]	val-χ^2 [e/Å^5]
ortho1	−0.042	4.37×10^{-3}	1.19×10^{-4}	-3.92×10^{-4}	1.01×10^{-4}	7.76×10^{-6}	1.30×10^{-5}
	−0.155	4.65×10^{-3}	1.68×10^{-4}	0	6.98×10^{-5}	1.07×10^{-5}	1.90×10^{-5}
	−0.126	4.15×10^{-3}	1.56×10^{-4}	0	0	1.43×10^{-5}	2.33×10^{-5}
meta2	−0.463	0	3.03×10^{-4}	1.24×10^{-4}	1.83×10^{-5}	4.99×10^{-7}	6.43×10^{-7}
	−0.363	5.51×10^{-4}	2.60×10^{-4}	0	0	5.93×10^{-7}	8.37×10^{-7}
	−0.388	0	2.71×10^{-4}	0	0	6.48×10^{-7}	7.62×10^{-7}
para3	−0.132	6.33×10^{-3}	1.59×10^{-4}	-4.15×10^{-4}	3.98×10^{-5}	7.58×10^{-7}	1.62×10^{-6}
	−0.162	6.39×10^{-3}	1.73×10^{-4}	-3.35×10^{-4}	0	8.46×10^{-7}	1.59×10^{-6}
	−0.422	6.03×10^{-3}	2.86×10^{-4}	0	0	1.06×10^{-6}	1.74×10^{-6}
meta4	−0.361	0	2.59×10^{-4}	-4.65×10^{-5}	9.38×10^{-6}	4.59×10^{-7}	6.82×10^{-7}
	−0.399	2.56×10^{-5}	2.75×10^{-4}	0	0	4.82×10^{-7}	7.47×10^{-7}
	−0.400	0	2.76×10^{-4}	0	0	4.82×10^{-7}	5.62×10^{-7}
ortho5	−0.071	4.00×10^{-3}	1.33×10^{-4}	0	-5.18×10^{-5}	3.38×10^{-6}	7.81×10^{-6}
	−0.032	4.47×10^{-3}	1.16×10^{-4}	-1.47×10^{-4}	0	3.68×10^{-6}	6.07×10^{-6}
	−0.082	4.59×10^{-3}	1.37×10^{-4}	0	0	4.35×10^{-6}	6.65×10^{-6}

TABLE 5: Parameters of the Best Fit Functions of the Ellipticities in the BCPs of Each ph−CH Bond[a]

Fits of ϵ(BCP) Based on Lowest ρ Convention and According to Eq *2*							
variables	1	σ^H	WN	IR	RA		
parameter	a	b	c	d	e	χ^2	val-χ^2
ortho1	−0.1181	-8.714×10^{-3}	5.918×10^{-5}	0	0	2.70×10^{-5}	3.58×10^{-5}
	−0.0512	-8.981×10^{-3}	3.043×10^{-5}	-2.087×10^{-4}	0	2.60×10^{-5}	4.24×10^{-5}
meta2	0.0174	0	0	0	-4.011×10^{-5}	1.99×10^{-6}	2.41×10^{-6}
	0.0540	5.726×10^{-4}	-1.700×10^{-5}	0	0	2.39×10^{-6}	3.52×10^{-6}
	0.2569	9.404×10^{-4}	-1.047×10^{-4}	-2.421×10^{-4}	0	2.24×10^{-6}	3.64×10^{-6}
para3	0.0187	-1.375×10^{-2}	0	5.894×10^{-4}	-1.503×10^{-4}	4.65×10^{-6}	7.47×10^{-6}
	0.3130	-1.358×10^{-2}	-1.302×10^{-4}	0	0	6.60×10^{-6}	1.05×10^{-5}
	−0.1843	-1.426×10^{-2}	8.485×10^{-5}	6.387×10^{-4}	0	5.85×10^{-6}	1.02×10^{-5}
meta4	0.2624	1.735×10^{-3}	-1.070×10^{-4}	-2.476×10^{-4}	0	1.08×10^{-6}	1.71×10^{-6}
	0.0705	1.437×10^{-3}	-2.418×10^{-5}	0	0	1.53×10^{-6}	2.17×10^{-6}
	0.2624	1.735×10^{-3}	-1.070×10^{-4}	-2.476×10^{-4}	0	1.08×10^{-6}	1.71×10^{-6}
ortho5	−0.2531	-9.309×10^{-3}	1.177×10^{-4}	0	0	2.51×10^{-5}	3.71×10^{-5}
	−0.3105	-9.167×10^{-3}	1.425×10^{-4}	1.707×10^{-4}	0	2.42×10^{-5}	4.42×10^{-5}

[a] The first row for each ph position contains parameters of the best fits for the respective ph position, and the two following rows contain parameter of the fits depending on $\sigma^H_{C_6H_6}$, WN, and $\sigma^H_{C_6H_6}$, WN, IR, respectively, leading to reliable fit-results.

TABLE 6: Parameters of the Best Fit Functions of ρ, $\nabla^2\rho$, or ϵ in the BCPs of Each ph−CH Bond Applying Relative Values for Each Spectroscopic Variable[a]

	Fits of ρ(BCP) - relative values					val-$\chi^2_{rel.}$	val-$\chi^2_{abs.}$	$SD_{rel.}$	$\Delta F_{rel.}$	
var.	1	σH	WN	IR	RA				min.	common
param.	a	b	c	d	e	[e/Å^3]	[e/Å^3]	[e/Å^3]	[e/Å^3]	[e/Å^3]
o1	0.276	1.79×10^{-3}	6.75×10^{-5}	-9.51×10^{-4}	1.24×10^{-3}	$\mathbf{2.02 \times 10^{-6}}$	2.02×10^{-6}	3.45×10^{-4}	2.21×10^{-6}	8.58×10^{-5}
m2	0.275	0	1.67×10^{-4}	7.14×10^{-4}	2.46×10^{-4}	$\mathbf{1.31 \times 10^{-7}}$	1.31×10^{-7}	8.78×10^{-5}	4.06×10^{-6}	1.68×10^{-4}
p3	0.277	2.73×10^{-3}	8.68×10^{-5}	-1.10×10^{-3}	0	$\mathbf{2.92 \times 10^{-7}}$	2.92×10^{-7}	1.31×10^{-4}	3.37×10^{-6}	1.13×10^{-4}
m4	0.276	0	1.39×10^{-4}	0	0	$\mathbf{1.13 \times 10^{-7}}$	1.13×10^{-7}	8.14×10^{-5}	2.78×10^{-6}	1.39×10^{-4}
o5	0.277	2.01×10^{-3}	5.86×10^{-5}	-5.51×10^{-4}	0	$\mathbf{2.57 \times 10^{-6}}$	2.57×10^{-6}	3.89×10^{-4}	2.63×10^{-6}	7.81×10^{-5}
	Fits of $\nabla^2\rho$(BCP) - relative values					[e/Å^5]	[e/Å^5]	[e/Å^5]	[e/Å^5]	[e/Å^5]
o1	0.230	4.37×10^{-3}	1.21×10^{-4}	-2.68×10^{-3}	5.10×10^{-3}	$\mathbf{1.28 \times 10^{-5}}$	1.30×10^{-5}	8.69×10^{-4}	4.15×10^{-6}	1.67×10^{-4}
m2	0.230	0	3.03×10^{-4}	8.39×10^{-4}	9.23×10^{-4}	$\mathbf{6.42 \times 10^{-7}}$	6.43×10^{-7}	1.94×10^{-4}	6.92×10^{-6}	3.05×10^{-4}
p3	0.235	6.39×10^{-3}	1.73×10^{-4}	-2.26×10^{-3}	0	$\mathbf{1.59 \times 10^{-6}}$	1.59×10^{-6}	3.06×10^{-4}	7.58×10^{-6}	2.34×10^{-4}
m4	0.232	0	2.76×10^{-4}	0	0	$\mathbf{5.62 \times 10^{-7}}$	5.62×10^{-7}	1.82×10^{-4}	5.52×10^{-6}	2.76×10^{-4}
o5	0.233	4.47×10^{-3}	1.16×10^{-4}	-9.95×10^{-4}	0	$\mathbf{6.07 \times 10^{-6}}$	6.07×10^{-6}	5.98×10^{-4}	5.78×10^{-6}	1.59×10^{-4}
	Fits of ϵ(BCP) - relative values									
o1	0.018	-8.71×10^{-3}	5.92E-05	0	0	$\mathbf{3.58 \times 10^{-5}}$	3.58×10^{-5}	1.45×10^{-3}	-7.53×10^{-6}	-2.80×10^{-5}
m2	0.017	0	0	0	-2.09×10^{-3}	$\mathbf{2.39 \times 10^{-6}}$	2.41×10^{-6}	3.75×10^{-4}	-2.09×10^{-8}	-2.09×10^{-6}
p3	0.019	-1.38×10^{-2}	0	4.11×10^{-3}	-7.70×10^{-3}	$\mathbf{7.41 \times 10^{-6}}$	7.47×10^{-6}	6.60×10^{-4}	-9.73×10^{-6}	-1.41×10^{-4}
m4	0.017	1.73×10^{-3}	−1.07E-04	-1.67×10^{-3}	0	$\mathbf{1.71 \times 10^{-6}}$	1.71×10^{-6}	3.17×10^{-4}	-2.08×10^{-6}	-9.14×10^{-5}
o5	0.017	-9.31×10^{-3}	1.18E-04	0	0	$\mathbf{3.71 \times 10^{-5}}$	3.71×10^{-5}	1.48×10^{-3}	-6.95×10^{-6}	2.46×10^{-5}

[a] The corresponding fit performance is estimated via the val-χ^2_{rel} or SD_{rel} values (val-χ^2_{abs} listed for comparison). The minimal and common uncertainties of the measures were regarded to estimate the errors of the predicted values due to imperfect input data for the fits ΔF_{rel}.

between ϵ(*meta*-CH BCP) of the benzene-derivatives, as shown in Figure 9. Nevertheless, the best fit function allows a precise classification of new ϵ(*para*-CH BCP) values in a set of known ϵ because the ϵ(*para*-CH BCP) values are covering a much larger range than for example ϵ(*meta*-CH BCP), as visualized in Figure 9. The three variables with the highest correlation coefficients concerning ϵ ($\sigma^{1H}_{C_6H_6}$, IR, RA) are also the ones leading to the lowest val-χ^2 values for linear fits.

Hence, one can conclude that on the basis of spectroscopic variables ϵ in CH BCPs of monosubstituted benzene derivatives can be well predicted. A constraint is only present for the meta positions, where the prediction accuracy is although high but is not sufficient to classify ϵ of comparable CH BCPs of new substances into a set of already studied benzene derivatives. This is due to the low differences between ϵ in the BCPs at the meta positions of the studied molecules (Figure 3).

Application of Relative Values. Relative values can be used to enhance the accuracy of the deployed quantity (even experimental) for predicting the target values ρ, $\nabla^2\rho$, or ϵ. In the case of the ^{1}H NMR shifts, relative values are already employed in the preceding sections. Additionally, we investigated the validity of the fits when using exclusively relative spectroscopic quantities, as relative wavenumbers (difference to the respective value of benzene), IR intensities, and Raman intensities (normalized to the benzene signals), whereas the latter were calculated from the Raman activities as described in the section "Calculation of Vibrational Data and NMR Shifts". As can be seen in Table 6, the fit-results are almost identical to the ones discussed previously (Tables 3−5). Nevertheless, the application of relative values is very promising with regard to the employment of accurate experimental spectroscopic data.

In this context, the precision of the experimentally determined spectroscopic variables is of crucial importance. Because the accuracy of such measures usually depends on the investigated system and the utilized setup, a minimal and a common error were estimated. The resulting total experimental error ΔF_{rel} is compared to the standard deviation of the fits SD_{rel} calculated from val-χ^2_{rel} as shown in Table 6. SD_{rel} and ΔF_{rel} were calculated according to eqs 6 and 7.

$$SD_{rel} = \sqrt{\frac{val - \chi^2}{n - 1}} \quad (6)$$

$$\Delta F = b\Delta\alpha + c\Delta\beta + d\Delta\gamma + e\Delta\delta \quad (7)$$

In eq 7, the quantities $\Delta\alpha$, $\Delta\beta$, $\Delta\gamma$, $\Delta\delta$ correspond to the measurement errors of the ^{1}H NMR shift, the wavenumber shift, the relative IR intensities, and Raman intensities, each with respect to benzene, and are weighted by the parameters of the fit model (Table 6). For the detection of ^{1}H NMR shifts, a minimum error of 0.001 ppm and a usual error of 0.01 ppm were assumed. In the case of vibrational spectroscopy, wavenumber shifts with an accuracy of about 1 cm^{-1} can be detected, whereas the sensitivity can be even enhanced to shifts of roughly 0.02 cm^{-1} by applying sophisticated difference setups.[88] The ratios of IR[89] as well as Raman bands are assumed to possess a minimum error of 0.001 for optimal conditions and a usual error of about 0.05.

As revealed by Table 6 and visualized in Figure 10, the estimated minimal uncertainties are 1−2 magnitudes lower than the standard deviations of the validated fits. Even the estimated uncertainties obtainable via standard measurements are of comparable scale as SD_{rel} or are even one magnitude lower. Hence, the application of the herein derived methodology can be reliably transferred to experimental values, whereas high-performance measurements should be applied if applicable. In particular, the exact determination of ^{1}H NMR and wavenumber shifts is a crucial task because even the exclusive application of these quantities leads to excellent val-χ^2_{rel} values (Tables 2−6).

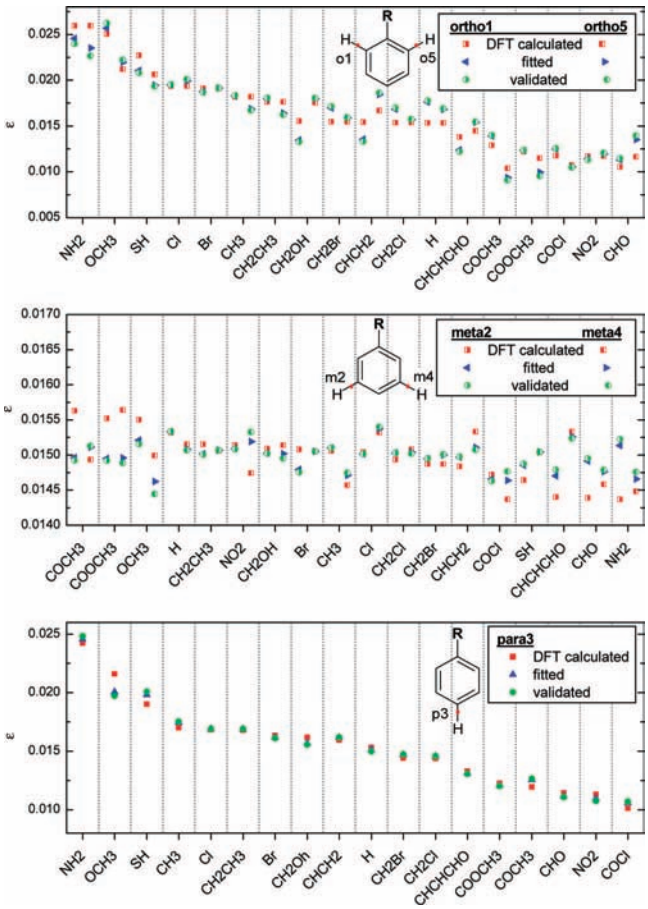

Figure 9. DFT-calculated, fitted, and validated ϵ values in the BCP of the CH bonds. The fit functions are linear and the parameters are the ones leading to the lowest val-χ^2 in Table 5.

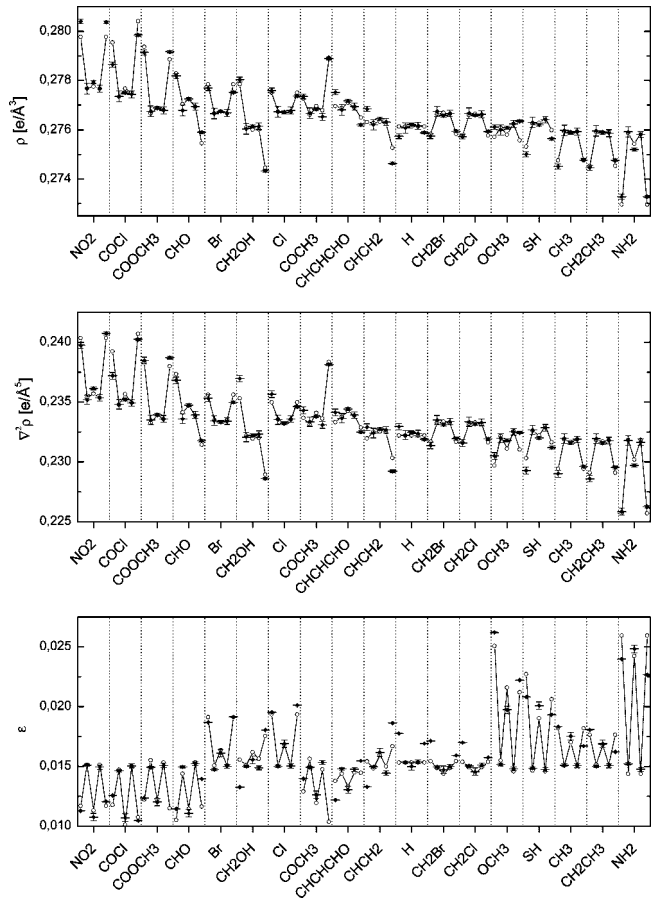

Figure 10. DFT-calculated (circles connected with lines) and validated (diamonds) target values (ρ, $\nabla^2\rho$, ϵ) in the BCPs of the *o1*-, *m2*-, *p3*-, *m4*-, *o5*-CH bonds (from left to right in each column), applying relative spectroscopic measures. The fit functions are linear and the parameters are those leading to the lowest val-χ^2 values presented in Table 6. Furthermore, experimental uncertainties were estimated and added as error bars to the predicted values. Minimal and common errors are indicated by black broad and by gray slender bars.

Conclusions. In this article, we presented a statistical approach to predict electron density properties in ph−CH bonds by means of vibrational and ^{1}H NMR data. All data are based on DFT calculations, whereas the electron density characteristics were supported by MP2 calculations. The prediction of electron density properties on the basis of spectroscopic data is of huge interest because it facilitates the investigation of the reactivity-determining electron-density distribution of substances in liquid states or in solvent environments, whereas the direct determination of the electron-density distribution is only possible in single crystals.

The electron-density-target quantities were chosen to be the electron density ρ, the respective laplacians $\nabla^2\rho$, and the ellipticity ϵ within the ph−CH bond critical points because they were found to be key characteristics in electrophilic substitution reactions. The quantities ρ, $\nabla^2\rho$, and ϵ were correlated with wavenumber values, IR intensities, and Raman activities of inherently localized CD-stretching vibrations and ^{1}H NMR shifts, using benzene as a reference. The vibrational data of the localized CD-stretching vibrations have proven to be well suited for correlations with electron-density properties of individual CH bonds, in contrast to parameters of normal modes involving substituent vibrations, for example in a set of benzene derivatives, which inherently differ. As expected, the spectroscopic quantities possessing high linear correlation coefficients con-

cerning ρ, $\nabla^2\rho$, or ϵ are also important variables in fit functions of ρ, $\nabla^2\rho$, and ϵ with the highest performance. These fit functions, best suited to predict ρ, $\nabla^2\rho$, and ϵ values, are involving wavenumber values and ^{1}H NMR data. The fits of the electron density, the laplacians, and the ellipticity allow for a classification of unknown ρ,$\nabla^2\rho$, and ϵ values of monosubstituted benzene derivatives. The prediction performance was evaluated by a validation procedure leading to validated sums over squared errors val-χ^2.

Further efforts have to be accomplished to generate experimental data sets. If electron density, vibrational, and NMR data are available, that is for crystalline monodeuterated benzene derivatives, the functions relating the electron density and the spectroscopic data can be adjusted. Thus, particular electron density features even of noncrystalline substances can be obtained from easily detectable vibrational and NMR spectroscopic data. Actually, changes in the electron density distribution during environment changes or chemical reactions might be traced. The anyhow varied spectroscopic input variables would directly output the changed electron density features.

To extend the described approach beyond utilizing naturally localized vibrations, the possibility of the pure experimental character of the method gets lost because the commonly known partitioning schemes to express the properties of normal modes in terms of internal coordinates have to be implemented. Furthermore, the applicability beyond particular classes of substances has to be investigated. However, we have shown in this article that CD-stretching vibrations in combination with ^{1}H NMR signals are a marker for crucial CH-bond properties.

Acknowledgment. We acknowledge the support by the Deutsche Forschungsgemeinschaft (Schwerpunktprogramm 1178).

Supporting Information Available: Graphs and figures of the correlation of vibrational data with electron density features based on localized CD stretching vibrations. This material is available free of charge via the Internet at http://pubs.acs.org.

References and Notes

(1) Hohenberg, P.; Kohn, W. *Phys. Rev. B: Solid State* **1964**, *136*, 864.
(2) Luger, P. *Org. Biomol. Chem.* **2007**, *5*, 2529.
(3) Henn, J.; Ilge, D.; Leusser, D.; Stalke, D.; Engels, B. *J. Phys. Chem. A* **2004**, *108*, 9442.
(4) Henn, J.; Leusser, D.; Stalke, D. *J. Comput. Chem.* **2007**, *28*, 2317.
(5) Messerschmidt, M.; Scheins, S.; Grubert, L.; Pätzel, M.; Szeimies, G.; Paulmann, C.; Luger, P. *Angew. Chem., Int. Ed.* **2005**, *44*, 3925.
(6) Eickerling, G.; Mastalerz, R.; Herz, V.; Scherer, W.; Himmel, H.-J.; Reiher, M. *J. Chem. Theory Comput.* **2007**, *3*, 2182.
(7) Hebben, N.; Himmel, H.-J.; Eickerling, G.; Herrmann, C.; Reiher, M.; Herz, V.; Presnitz, M.; Scherer, W. *Chem.−Eur. J.* **2007**, *13*, 10078.
(8) Grabowsky, S.; Pfeuffer, T.; Checinska, L.; Weber, M.; Morgenroth, W.; Luger, P.; Schirmeister, T. *Eur. J. Org. Chem.* **2007**, 2759.
(9) Flaig, R.; Koritsanszky, T.; Soyka, R.; Häming, L.; Luger, P. *Angew. Chem., Int. Ed.* **2001**, *40*, 355.
(10) Hibbs, D. E.; Austin-Woods, C. J.; Platts, J. A.; Overgaard, J.; Turner, P. *Chem.−Eur. J.* **2003**, *9*, 1075.
(11) Jelsch, C.; Pichon-Pesme, V.; Lecomte, C.; Aubry, A. *Acta Crystallogr. Sect. D* **1998**, *D54*, 1306.
(12) Housset, D.; Benabicha, F.; Pichon-Pesme, V.; Jelsch, C.; Maierhofer, A.; David, S.; Fontecilla-Camps, J. C.; Lecomte, C. *Acta Crystallogr., Sect. D* **2000**, *D56*, 151.
(13) Dittrich, B.; Koritsanszky, T.; Luger, P. *Angew. Chem., Int. Ed.* **2004**, *43*, 2718.
(14) Pichon-Pesme, V.; Jelsch, C.; Guillot, B.; Lecomte, C. *Acta Crystallogr., Sect. A* **2004**, *A60*, 204.
(15) Volkov, A.; Li, X.; Koritsanszky, T.; Coppens, P. *J. Phys. Chem. A* **2004**, *108*, 4283–4300.
(16) Pichon-Pesme, V.; Lecomte, C.; Lachekar, H. *J. Phys. Chem.* **1995**, *99*, 6242.
(17) Matta, C. F.; Bader, R. F. W. *Proteins: Struct., Funct., Genet.* **2002**, *40*, 310.
(18) Matta, C. F.; Bader, R. F. W. *Proteins: Struct., Funct., Genet.* **2003**, *52*, 360.
(19) Matta, C. F.; Bader, R. F. W. *Proteins: Struct., Funct., Genet.* **2000**, *40*, 310.
(20) Mebs, S.; Messerschmidt, M.; Luger, P. *Z. Kristallogr.* **2006**, *221*, 656.
(21) Meister, J.; Schwarz, W. H. E. *J. Phys. Chem.* **1994**, *98*, 8245.
(22) Kagiya, T.; Sumida, Y.; Inoue, T. *Bull. Chem. Soc. Jpn.* **1968**, *41*, 767.
(23) Hammett, L. P. *Phys. Org. Chem.* **1940**, *59*, 96.
(24) Suschtschinskij, M. M. *Ramanspektren von Molekülen und Kristallen*; Heyden & Son GmbH: Rheine, 1974.
(25) Jaffe, H. H. *Chem. Rev.* **1953**, *53*, 191.
(26) Hansch, C.; Leo, A.; Taft, R. W. *Chem. Rev.* **1991**, *91*, 165.
(27) Emsley, J. W. *J. Chem. Soc., A* **1968**, 2018.
(28) Tino, J.; Klimo, V. *J. Mol. Struct.* **1977**, *39*, 139.
(29) Dailey, B. P.; Gawer, A.; Neikam, W. C. *Discuss. Faraday Soc.* **1962**, *34*, 18.
(30) Kanekar, C. R.; Govil, G.; Khetrapal, C. L. *Proceedings - Indian Academy of Sciences, Section A* **1967**, *65*, 353.
(31) Brownlee, R. T. C.; Katritzky, A. R.; Sinnott, M. V.; Szafran, M.; Yakhontov, L. N.; Topsom, R. D. *Tetrahedron Lett.* **1968**, *9*, 5773.
(32) Brownlee, R. T. C.; Katritzky, A. R.; Topsom, R. D. *J. Am. Chem. Soc.* **1965**, *87*, 3260.
(33) Brownlee, R. T. C.; Katritzky, A. R.; Topsom, R. D. *J. Am. Chem. Soc.* **1966**, *88*, 1413.
(34) Brownlee, R. T. C.; Hutchinson, R. E. J.; Katritzky, A. R.; Tidwell, T. T.; Topsom, R. D. *J. Am. Chem. Soc.* **1968**, *90*, 1757.
(35) Schmid, E. D. *Spectrochim. Acta* **1966**, *22*, 1659.
(36) Schmid, E. D.; Hoffmann, V. *Spectrochim. Acta* **1966**, *22*, 1633.
(37) Schmid, E. D.; Hoffmann, V.; Joeckle, R.; Langenbucher, F. *Spectrochim. Acta* **1966**, *22*, 1615.
(38) Schmid, E. D.; Joeckle, R. *Spectrochim. Acta* **1966**, *22*, 1645.
(39) Schmid, E. D.; Langenbucher, F. *Spectrochim. Acta* **1966**, *22*, 1621.
(40) Taft, R. W. J. *Steric Effects in Organic Chemistry*; John Wiley and Sons: New York, 1956.
(41) Palat, K., Jr.; Waisser, K.; Exner, O. *J. Phys. Org. Chem.* **2001**, *14*, 677.
(42) Bobovich, J. S. *Optika i Spektroskopija* **1965**, *19*, 886.
(43) Bobovich, J. S. *Optika i Spektroskopija* **1966**, *20*, 252.
(44) Bobovich, J. S. *Optika i Spektroskopija* **1966**, *20*, 68.
(45) Bobovich, J. S.; Beljajewskaja, N. M. *Optika i Spektroskopija* **1965**, *19*, 198.
(46) Bader, R. F. W. *Atoms in Molecules: A Quantum Theory*; Oxford University Press: New York, 1990.
(47) Bader, R. F. W.; Chang, C. *J. Phys. Chem.* **1989**, *93*, 2946.
(48) Bader, R. F. W.; MacDougall, P. J. *J. Am. Chem. Soc.* **1985**, *107*, 6788.
(49) Hernandes-Trujillo, J.; Bader, R. F. W. *J. Phys. Chem. A* **2000**, *104*, 1779.
(50) Rode, J. E.; Dobrowolski, J. C. *Chem. Phys. Lett.* **2007**, *449*, 240.
(51) Lopez, C. S.; Faza, O. N.; Cossio, F. P.; York, D. M.; de Lera, A. R. *Chemistry* **2005**, *11*, 1734.
(52) Presselt, M.; Dietzek, B.; Schmitt, M.; Winter, A.; Chiper, M.; Friebe, C.; Schubert, U. S.; Popp, J. *J. Phys. Chem. C* **2008**, submitted.
(53) Mulliken, R. S. *J. Chem. Phys.* **1955**, *23*, 2343.
(54) Mulliken, R. S. *J. Chem. Phys.* **1955**, *23*, 2338.
(55) Mulliken, R. S. *J. Chem. Phys.* **1955**, *23*, 1841.
(56) Mulliken, R. S. *J. Chem. Phys.* **1955**, *23*, 1833.
(57) Messerschmidt, M.; Wagner, A.; Wong, M. W.; Luger, P. *J. Am. Chem. Soc.* **2002**, *124*, 732.
(58) Herrmann, C.; Reiher, M.; Hess, B. A. *J. Chem. Phys.* **2005**, 122.
(59) Gomes, T. C. F.; Viçozo da Silva, J., Jr.; Vidal, L. N.; Vazquez, P. A. M.; Bruns, R. E. *Theor. Chem. Acc.* 2008.
(60) Frisch, M. J. Schlegel, G. W. T., B. Scuseria, G. E. Robb, M. A. Cheeseman, J. R. Montgomery, J. A., Jr., Vreven, T. Kudin K. N. and Burant, J. C. Millam, J. M. Iyengar, S. S. Tomasi, J. Barone, V. Mennucci, B. Cossi, M. Scalmani, G. Rega, N. Petersson, G. A. Nakatsuji, H. Hada, M. Ehara, M. Toyota, K. Fukuda, R. Hasegawa, J. Ishida, M. Nakajima, T. Honda, Y. Kitao, O. Nakai, H. Klene, M. Li, X. Knox, J. E. Hratchian, H. P. Crossand, J. B. Adamo, C. Jaramillo, J. Gomperts, R. Stratmann, R. E. Yazyev, O. Austin, A. J. Cammi, R. Pomelli, C. Ochterski, J. W. Ayala, P. Y. Morokuma, K. Voth, G. A. Salvador, P. Dannenberg, J. J. Zakrzewski, V. G. Dapprich, S. Daniels, A. D. Strain, M. C. Farkas, O. Malick, D. K. Rabuck, A. D. Raghavachari, K. Foresman, J. B. Ortiz, J. V. Cui, Q. Baboul, A. G. Clifford, S. Cioslowski, J. Stefanov, B. B. Liu, G. Liashenko, A. Piskorz, P. Komaromi, I. Martin, R. L. Fox, D. J. Keith, T. Al-Laham, M. A. Peng, C. Y. Nanayakkara, A. Challacombe, M. Gill, P. M. W. Johnson, B. Chen, W. Wong, M. W. Gonzalez, C. Pople. J. A. *Gaussian 03*; Revision B.04; Gaussian, Inc.: Pittsburgh PA, 2003.
(61) Becke, A. D. *Phys. Rev. A* **1988**, *38*, 3098.
(62) Perdew, J. P. *Phys. Rev. B* **1986**, *33*, 8822.
(63) Schaefer, A.; Horn, H.; Ahlrichs, R. *J. Chem. Phys.* **1992**, *97*, 2571.

(64) Schaefer, A.; Huber, C.; Ahlrichs, R. *J. Chem. Phys.* **1994**, *100*, 5829.
(65) Herrmann, C.; Neugebauer, J.; Presselt, M.; Schmitt, M.; Rau, S.; Popp, J.; Reiher, M. *J. Phys. Chem. B* **2007**, *111*, 6078.
(66) Reiher, M.; Brehm, G.; Schneider, S. *J. Phys. Chem. A* **2004**, *108*, 734.
(67) Moller, C.; Plesset, M. S. *Phys. Rev.* **1934**, *46*, 618.
(68) Clark, T.; Chandrasekhar, J.; Spitznagel, G. W.; Schleyer, P. v. R. *J. Comput. Chem.* **1983**, *4*, 294.
(69) Krishnan, R.; Binkley, J. S.; Seeger, R.; Pople, J. A. *J. Chem. Phys.* **1980**, *72*, 650.
(70) McLean, A. D.; Chandler, G. S. *J. Chem. Phys.* **1980**, *72*, 5639.
(71) Binning, R. C., Jr.; Curtiss, L. A. *J. Comput. Chem.* **1990**, *11*, 1206.
(72) Curtiss, L. A.; McGrath, M. P.; Blaudeau, J.-P.; Davis, N. E.; Binning, R. C., Jr.; Radom, L. *J. Chem. Phys.* **1995**, *103*, 6104.
(73) McGrath, M. P.; Radom, L. *J. Chem. Phys.* **1991**, *94*, 511.
(74) Biegler-König, F.; Schönbohm, J. *J. Comput. Chem.* **2001**, *22*, 545.
(75) Biegler-König, F.; Schönbohm, J. *AIM2000*, 2.0 ed.; 2002.
(76) Ochterski, J. Vibrational Analysis in Gaussian. In *Gaussian White Papers*, 1999.
(77) Schrader, B. Infrared and Raman Spectroscopy; VCH Publishers: New York, 1995.
(78) Schrötter, H. W.; Klöckner, H. W. *Raman Scattering Cross-Sections in Gases and Liquids*; Springer-Verlag: Berlin, 1979.
(79) London, F. *Journal de Physique et Le Radium* **1937**, *8*, 397.
(80) McWeeny, R. *Phys. Rev.* **1962**, *126*, 1028.
(81) Ditchfield, R. *Mol. Phys.* **1974**, *27*, 789.
(82) Dodds, J. L.; McWeeny, R.; Sadlej, A. J. *Mol. Phys.* **1980**, *41*, 1419.
(83) Wolinski, K.; Hilton, J. F.; Pulay, P. *J. Am. Chem. Soc.* **1990**, *112*, 8251.
(84) Gutmann, T.; Schweitzer, A.; Wächtler, M.; Breitzke, H.; Buchholz, A.; Plass, W.; Buntkowsky, G. *Z. Phys. Chem.* **2008**, *222*, 1389.
(85) Schweitzer, A.; Gutmann, T.; Wächtler, M.; Breitzke, H.; Buchholz, A.; Plass, W.; Buntkowsky, G. *Solid State Nucl. Magn. Reson.* **2008**, *34*, 52.
(86) Danzer, K.; Hobert, H.; Fischbacher, C.; Jagemann, K.-U. *Chemometrik - Grundlagen und Anwendungen*; Springer: Berlin, 2001.
(87) Bronstein, I. N.; Semendjajew, K. A.; Musiol, G.; Mühlig, H. *Taschenbuch der Mathematik*; Verlag Harri Deutsch: Thun und Frankfurt, 2001.
(88) Frosch, T.; Meyer, T.; Schmitt, M.; Popp, J. *Anal. Chem.* **2007**, *79*, 6159.
(89) Ivanovski, V.; Mayerhöfer, T.; Popp, J. *Vib. Spectrosc.* **2008**, *47*, 91.

JP809601A